Upconverting Nano-engineered Surfaces: Maskless Photolithography for Security Applications

Fatemeh Kaboli,[a,b] Nahid Ghazyani,[a,b] Mohammadreza Riahi,[c] Hossein Zare-Behtash,[d] Mohammad Hossein Majles Ara,[a,b] Esmaeil Heydari,*[a,b]

[a]Faculty of Physics, Kharazmi University, Tehran, Iran

[b]Applied Science Research Center, Kharazmi University, Tehran, Iran

[c]Faculty of Physics, K. N. Toosi University of Technology, Tehran, Iran

[d]Aerospace Sciences Division, School of Engineering, University of Glasgow, Glasgow, UK

*Email: e.heydari@khu.ac.ir

Abstract

The two complementary technologies of colloidal upconverting nano-emitters and maskless photolithography are exploited to fabricate nano-engineered optically-active surfaces for anti-counterfeiting applications based on multipho1ton absorption phenomenon in lanthanide nanocomposites with a visualization wavelength in the NIR. It is demonstrated that the unique optical, thermal, and temporal characteristics of these versatile upconverting surface distinguishes them from their counterparts. A unique behaviour that is captured is the ability to actively tune their emission color by modifying the pumping power, temperature, and excitation frequency. A new low-cost negative photoresist is employed for implementation of maskless photolithography of single and double-color labels using two efficient upconverting nanocomposites based on $NaYF4:Yb^{3+},Er^{3+}$ and $NaYF4:Yb^{3+},Tm^{3+}$ nano-emitters. What's more, it is shown that the detectability of the proposed anti-counterfeiting approach can be carried out using just a smartphone. Each of the emission peaks of the upconversion nanoparticles is associated with a different multiphoton absorption mechanism and their thermosensitivity varies from one peak to another. Furthermore, their photoluminescent color changes by scanning the excitation beam impinging on the surfaces comprised of both upconversion nanoparticles doped in the UV-curable resist. Longterm photostability of these surfaces under continuous excitation by a high power laser makes them a promising nano-emitters for the next generation of anti-counterfeiting labels

Keywords

Upconversion nano-emitters, Anti-counterfeiting, Maskless photolithography, Photoresist, Photoluminescence, Multiphoton absorption

Introduction

Counterfeit cash is a worldwide epidemic, causing major headaches for economies around the globe. Countries are losing large amounts of investments annually as a result of counterfeiting. Thus, developing advanced anti-counterfeiting technologies as an alternative to current anti-counterfeiting approaches is in high demand. Over the past decades, Lanthanide-doped upconversion nanoparticles (UCNPs) have found tremendous potential in applications such as photoluminescent materials since the first observation of the upconversion phenomenon. This attraction is because of the narrow bandwidth emission in the ultraviolet (UV) and visible (Vis) spectrum under near infra-red (NIR) excitation. [1, 2, 3] Emission in nature is dominantly down conversion (DC) where the energy of the emitted photon is smaller than the excitation photon. However, in UC emission a high energy photon is created as a result of several low energy photons. One of the challenges in dealing with Lanthanide-doped UCNPs is their low quantum yield. In 1972, $NaYF_4:Yb^{3+},Er^{3+}$ was introduced as an efficient UC photoluminophore with a green emission. [4] Recently, $NaYF_4:Yb^{3+},Tm^{3+}$ has been found to be a high efficiency upconversion photoluminophore with multiple blue light emission bands. [5, 6, 7] Over the years, different methods have been successfully adopted based on thermal decomposition for efficient synthesising of UCNPs. [8, 9, 10] Lanthanide ions (Ln^{3+}) exhibit optical properties such as a narrow bandwidth emission as a result of 4f-5d and intra-4f transitions, anti-Stokes shift and longterm emission stability and lifetime. In the Lanthanide ions the 4f electrons are shielded by the filled $5s^2$ and $5p^6$ orbitals, therefore such transitions lead to weak electron-photon coupling and narrow bandwidth of Lanthanide-doped UCNPs. Another advantage of the Lanthanide-doped UCNPs is their size and environment-independent emission which avoids the creation of a wide spectrum and makes them distinctive from their counterparts such as organic dyes and quantum dots. This property is conferred from the fact that the emission wavelength is intrinsically determined by the 4f energy levels of the activators which is shielded by the occupied outer orbitals. In addition, the Lanthanide ions can emit in both single- and multi-photon excitation regimes where they are able to convert the NIR excitation light into Vis and UV emissions. Moreover, they exhibit long lifetimes resulting from the low transition probability of parity forbidden transitions. These attractive optical properties of UCNPs have therefore attracted great interest for their application in optical imaging, drug industries, food packaging, photo-dynamics therapy, optical sensors, lasers, solar cells, display devices, credit cards, and security inks. [11, 12]

Traditional anti-counterfeiting technologies, such as radio-frequency identification (RFID), quick response (QR) codes, and holography suffer from high cost, easy infringement, and even complex manufacturing processes. In the past, optically active QR codes were developed based on photoluminophores, plasmonic nanoparticles, and quantum dots in order to overcome the aforementioned drawbacks[13] necessitating the access to well established decoding procedures. However, the lack of longterm photostability, rapid photobleaching, interference of excitation and emission due to the small Stokes shift and the wide FWHM of their emission spectrum limits their applications. Instead, optically active security labels and QR codes based on UCNPs are a promising candidate.[14, 15] Recently, different printing technologies such as inject printing,[16, 17] mask photolithography, and aerosol jet printing have been used for patterning of the UCNPs.[18] Here, we integrate the mature science of colloidal UC nano-emitters, fast maskless photolithography together

with low cost UV-curable resist technologies to develop versatile, optically active and nano-engineered security surfaces with the ability of being excited with a 980 nm NIR laser light and revealed using nothing more than a smartphone. In addition, the optical, thermal and temporal characteristics of these optically active surfaces will be investigated and compared for two common UCNPs owing to their photostability, unique thermal, temporal and multi-photon characteristics, NIR excitation, multi-color emission, hardship in duplicating the UCNPs and NIR sources.

Results and Discussion

The two efficient UCNPs of $NaYF_4:Yb^{3+},Tm^{3+}$ and $NaYF_4:Yb^{3+},Er^{3+}$ were synthesized using the thermal decomposition method as nano-emitters for the current work.[19-26] Their properties were thoroughly investigated and compared before any applications. These UCNPs convert a continuous NIR light at a single-wavelength to several bands in the UV-Vis optical spectrum. In these UCNPs, the $NaYF_4$ host is doped with Yb^{3+} ions as sensitizer to transfer two or more NIR excitation photons to the Tm^{3+} or Er^{3+} ions as activator and subsequently emit one photon in the Vis or UV spectrum. Yb^{3+} ions are excellent for transferring energy to Er^{3+} ions because they have a single excited state for accumulating the excitation energy. Upon excitation with a 980 nm NIR diode laser beam, the Yb^{3+} is excited to the higher state of $^2F_{5/2}$ and non-radiatively transfers its energy to the excited state of Tm^{3+} or Er^{3+} which subsequently depopulates radiatively. Figure 1a depicts the absorption spectrum of the $NaYF_4:Yb^{3+},Tm^{3+}$ UCNPs. Maximum absorption is located at 978 nm which is associated with the absorption band of the Yb^{3+} sensitizer ions. The wavelength of the excitation beam is shown with a black dashed line at 980 nm. A similar spectrum was observed for $NaYF_4:Yb^{3+},Er^{3+}$ UCNPs. A TEM measurement was performed to acquire information regarding the size distribution of the UCNPs. The TEM image of the $NaYF_4:Yb^{3+},Tm^{3+}$ UCNPs with a maximum distribution at 15 nm is presented in the inset of Figure 1a. The TEM images clearly shows the nanoscale distribution of UCNPs.

The photoluminescence (PL) spectra of both colloidal solution of UCNPs in Hexane are shown in Figure 1b. PL of $NaYF_4:Yb^{3+},Er^{3+}$ and $NaYF_4:Yb^{3+},Tm^{3+}$ UCNPs, and the corresponding electronic transitions, are indicated in green and blue, respectively. The $NaYF_4:Yb^{3+},Er^{3+}$ UCNPs appear in a green-yellow color when they are excited with the 980 nm laser light and have multiple narrow emission bands with peaks at 408 nm, 525 nm, 541 nm, and 654 nm in the visible optical spectrum. For these UCNPs, the $^2F_{5/2}$ state of Yb^{3+} ions overlaps with the $^4I_{11/2}$ of Er^{3+} ions, thus Er^{3+} ions are excited to $^4F_{7/2}$ by two consecutive energy transfers from Yb^{3+} ions before transition to $^4I_{15/2}$ ground state takes place. Therefore, the green-yellow and red color emissions correspond to the transitions from $^2H_{11/2}$, $^4S_{3/2}$ and $^4F_{9/2}$ states to the ground state of $^4I_{15/2}$, respectively. PL of $NaYF_4:Yb^{3+},Tm^{3+}$ UCNPs appears in a blue color and have spectral emission bands with peaks at 345 nm, 362 nm, 451 nm, 475 nm, and 648 nm in the visible spectrum and 694 nm and 800 nm (not shown) in the NIR spectrum. Emissions at 345 nm, 362 nm, and 451 nm are associated with four-photon absorption in $^1I_6$ to $^3F_4$, $^1D_2$ to $^3H_6$, and $^1D_2$ to $^3F_4$ transitions. However, the blue emission at 475 nm results from a three-photon transition from the $^1G_4$ state to the $^3H_6$ state. Red emissions are caused by a two-photon absorption process.[27] Therefore , these two UCNPs can be used to generate green-yellow, blue, and when they are mixed together white colors as presented in the inset of figure 1b.

UV-curable resist Loxeal 3020 was used as a new low-cost matrix for patterning of the UCNPs. Loxeal 3020 is transparent in the visible spectrum and exhibits optical properties suitable for UCNPs. 38 mg/ml colloidal solutions of UCNPs in hexane were mixed in the resist matrix with a volume ratio of 1:2. It was then kept in a desiccator for 24 h to remove any solvent. The PL response of both UCNPs excited under different laser powers from 0.1 W to 2.6 W are compared in Figures 1c and 1d. The slope of PL intensity versus the laser excitation power for both peaks of NaYF4:Yb^{3+},Er^{3+} colloidal solution at 541 nm and 654 nm is constant and similar in the measured pumping range presented in figure 1c. The green squares are associated with the development of the green emission peak at 541 nm and the red circles with the red emission peak at 654 nm. This implies the presence of a uniform two-photon process for the measurement peaks. A similar two-photon absorption behavior was observed for the NaYF4:Yb^{3+},Er^{3+} UCNPs doped in the UV-cured resist which is not shown here. Inset in figure 1c shows the development of the PL by increasing the excitation pump power. Figure 1d shows the PL intensity of NaYF4:Yb^{3+},Tm^{3+} UCNPs in both the hexane and the UV-cured resist. The blue circles are associated with the development of the emission peak at 451 nm and green triangles with the emission at 475 nm. It is clear that the slope of the graph is not constant over the entire measurement region for the emission at 451 nm, and it deviates from a four-photon absorption for low pumping powers in both hexane and photoresist due to the insufficient power received for this transition to take place. A similar nonlinear trend was recorded for emission at 475 nm, which presents a three-photon absorption process. PL of the nanocomposites, shown by the half-filled red circles and black triangles, slightly deviate from the colloidal UCNPs. Figure 1e shows the corresponding logarithmic graph of figure 1c and 1d. Figure 1f illustrates the CIE1931 chromaticity diagram of both UCNPs doped in the photoresist matrix. Both the x and y coordinate of NaYF4:Yb^{3+},Er^{3+} UCNPs increase by raising the excitation pump power, which are shown with black dots on the right-hand side, while for NaYF4:Yb^{3+},Tm^{3+} UCNPs, which are shown to the left of the figure, the x coordinate decreases and y increases. The white arrow demonstrates the color change by raising the excitation power of NaYF4:Yb^{3+},Er^{3+} UCNPs and the black arrow indicates the color change by increasing the excitation power of NaYF4:Yb^{3+},Tm^{3+} UCNPs.

Figures 2a, 2b, 2c and 2d demonstrate the thermal response of both NaYF4:Yb^{3+}, Er^{3+} and NaYF4:Yb^{3+},Tm^{3+} UCNPs doped in the UV-cured resist when they are excited with a 300 mW excitation laser beam with a cross-section of 36 mm2. The results show that the PL of the NaYF4:Yb^{3+},Er^{3+} UCNPs are highly temperature dependent while the NaYF4:Yb^{3+},Tm^{3+} UCNPs exhibits minor temperature sensitivity in the UV-Vis range. Figure 2a depicts the change of the PL during a temperature variation in the range of 25°C to 75°C. The red triangles represent the peak position of the PL of NaYF4:Yb^{3+},Er^{3+} UCNPs at 408.3 nm associated with 2H9/2 to 4I15/2 transition. This remains constant until 40°C and then begins to decrease beyond this temperature. The blue triangles depict the peak position of the PL for decreasing the temperature. The overall change of intensity is less than 0.1. Figure 2b shows the PL intensity based on temperature for the peak at 541 nm associated with 4S3/2 to 4I15/2 transition. For this peak, a larger reduction of the PL intensity, in the order of 0.9, is observed. Again, the intensity stays constant until 40°C and decreases for higher temperatures up to 75°C. Different intensities were observed for cooling and heating, however at 25°C the intensities overlap. A similar behavior was observed for the peak at 654.4 nm, associated with the 4F7/2 to 4I15/2 transition in figure 2c, however the total change in

the intensity was 0.7. This reduction in the PL intensity is attributed to the phonon-assisted de-excitation at higher temperatures in NaYF4:Yb^{3+},Er^{3+} UCNPs. Comparison of the results reveals that the peak at 541.1 nm exhibits the largest intensity change in the defined range of temperature and is repeatable. It is due to the advantageous thermal behavior of the Er^{3+} transitions in these UCNPs that they are used in nanophotonic thermometry.28-33 An investigation was also carried out for the NaYF4:Yb^{3+},Tm^{3+} UCNPs in the UV-cured resist and minor variation in the PL intensity was observed as presented in figure 2d. The minor increase in intensity at high temperatures is attributed to the thermal population of the higher transition state induced by phonons. Figure 2e depicts the CIE1931 chromaticity diagram for both nanocomposites when the temperature was changed. Changes associated with NaYF4:Yb^{3+},Er^{3+} UCNPs are more considerable than NaYF4:Yb^{3+},Tm^{3+} UCNPs. In the case of the NaYF4:Yb^{3+},Er^{3+} based nanocomposite, the x coordinate decreases while the y coordinate increases when the temperature is raised from 25°C to 75°C. For the NaYF4:Yb^{3+},Tm^{3+} nanocomposite there is almost no color change observed.

The long term photostability of the two upconversion nanocomposites was investigated through continuous excitation of two samples under 300 mW power and 36mm2 laser cross section for 1 h at the room temperature. Figure 3 shows the magnitude of their PL intensities over a time span of 1h. The blue squares represent the PL of the nanocomposite based on NaYF4:Yb^{3+},Tm^{3+} UCNPs at 451 nm, and the green circles depict the nanocomposite based on NaYF4:Yb^{3+},Er^{3+} UCNPs at 541.1 nm. The black triangles show the excitation laser intensity captured every 5 minutes. PL reduction in the order of 9% was observed for the NaYF4:Yb^{3+},Er^{3+} UCNPs. On the other hand, a 2% increase was recorded for the NaYF4:Yb^{3+},Tm^{3+} UCNPs for the same time period. These changes are attributed to the thermal effects induced by the excitation laser, discussed earlier, since the pattern of the observed behavior is consistent with what was measured in the thermal experiments. In this figure, intensities can not be compared and are solely used to demonstrate the PL stability.

Maskless photolithography was used for the fabrication of different transparent patterns onto the nanocomposites comprising of UV-curable photoresist doped with UCNP nano-emitters. This is a fast, simple, and affordable technique for fabrication of different patterns based on the developed nanocomposites. This technique requires fewer steps than conventional photolithography techniques since it does not require any preparation of the photomask, and the optical projectors are affordable, easily accessible, and the projection is performed without any intermediate medium. For this purpose, a Primer 7 was used to modify a clean glass surface and enhance the adhesion of the UV-3020-based nanocomposite to the surface. Subsequently, 500 μL of transparent nanocomposite was injected onto a clean glass substrate. It was kept for few minutes in a vacuumed desiccator to remove any created bubbles and allow the nanocomposite spreads uniformly over the entire substrate.

Then the image of the designed pattern was projected onto its surface, which was located 5 cm away from the projector, for a time span of 20 s required for photocuring. After the curing, the sample was developed by quick washing with an abundant amount of acetone for 1 minute. The sample was then quickly washed with isopropanol at room temperature and dried with a nitrogen gun. The acetone dissolves the unexposed area without impacting the exposed area. Different techniques have been used by others for the printing of UCNPs. Figure 4 illustrates the maskless

photolithography setup relying on an Vivitek-DLP optical projector employed for pattering of the upconversion nanocomposite surfaces.

The detection setup is shown in figure 5a, which includes a 980 nm continuous NIR laser for excitation of the UCNPs based nanocomposite surface, a convex lens with a 30 cm focal length for focusing the laser beam onto the samples, and a set of perpendicular scanning galvo mirrors for fast sweeping of the focused light over the entire sample surface. The sweeping frequency was set by a signal generator. The initial spot size of the excitation laser is 36 mm^2 that becomes less than 1 mm^2 when it is pinging the samples. Combination of two galvo scanner mirrors enabled the excitation of large area samples. A smartphone was used to capture the PL image of all the samples in combination with a convex lens with a 5 cm focal length. Figure 5b depicts the PL image of a portrait of Kharazmi (Al-Khwarizmi), when it was excited with a 1W@36 mm^2 laser light, scanned with mirrors at a frequency of 500 Hz. In this sample, the nanocomposite only contains $NaYF_4:Yb^{3+},Er^{3+}$ UCNPs. Low power lasers can be used for surfaces comprising higher concentrations of UCNPs. This is important for the commercial applications. Figure 5c and 5d are associated with a nanocomposite comprising of a blend of two UCNPs. Interestingly, the QR-code sample appeared in a white color in figure 5c when the scanning galvo mirrors were turned off, as it was shown earlier in the inset of figure 1b, and switched to a green color when the entire sample was scanned with the oscillating mirrors at 1 kHz. We attribute this color tuning pattern to different lifetimes of the UCNPs contributing to color generation.[34, 35] This is a simple method to switch the color from white to green. Figure 5d shows the blue PL image of the logo of the Kharazmi University containing only $NaYF_4:Yb^{3+},Tm^{3+}$ UCNPs. Figure 5f is a QR-code image and figure 5h is a portrait of Ibn Al-haytham, containing $NaYF_4:Yb^{3+},Er^{3+}$ UCNPs. Figure 5g illustrates a two-color image including both UCNPs. In this case, the yellow-colored pattern was first fabricated based on the nanocomposite of $NaYF_4:Yb^{3+},Er^{3+}$ UCNPs and, in the second step after developing it, the blue-colored pattern was fabricated based on the $NaYF_4:Yb^{3+},Tm^{3+}$ UCNPs. The appeared lines are the scanning paths of the NIR laser beam. The exciting point about this configuration is that the surface is uniform and the pattern is unrecognizable until the laser beam is projected onto the surface.

Conclusions

There is an ever growing demand to develop advanced counterfeiting surfaces for a wide-range of commercial applications such as currencies, credit cards and security labels. The drawback of existing methods are the associated high costs, ease of duplication and re-writing. A versatile, fast, low-cost and facile technology based on the integration of two complementary technologies of colloidal upconversion nanotechnology and maskless photolithography has been demonstrated for the fabrication of nanoengineered surfaces for security applications. Two UCNPs of $NaYF_4:Yb^{3+},Er^{3+}$ and $NaYF_4:Yb^{3+},Tm^{3+}$ were used as green-yellow and blue nanoemitters, respectively. The optical, thermal, and temporal behavior of these nanoparticles were investigated to identify and validate their unique characteristics for security applications. It was demonstrated that the PL color can be changed with booth dynamic and static excitation. Implementation of security surfaces were performed in the context of single and double color patterns to prove the functionality of the UCNPs.

Methods

UCNPs Synthesis. For synthesis of NaYF4:Yb,Tm, firstly acetate hydrate salts of Y(1.4 mmol), Yb (0.6 mmol) and Tm (0.01 mmol) were mixed with oleic acid and octadecene and heated to a temperature of 120°C under vacuum conditions and then cooled down to 50°C. A solution containing NaOH and NH4F in methanol was added to the mentioned solution and stirred. The solution was slowly heated to a temperature of 120°C to evaporate the methanol and then heated at a fast rate to 300°C and maintained at this temperature for 1.5 h under argon gas. Afterwards, the solution was cooled down to room temperature, and the NaYF4:Yb,Tm nanoparticles were precipitated by addition of ethanol. They were then collected by centrifugation at 6000 rpm, washed with ethanol twice, and re-dispersed in hexane. Synthesis of NaYF4:Yb, Er nanocrystals was the same as NaYF4:Yb, Tm nanocrystals with different concentrations of 20 % and 2 % for Yb, Er, respectively. All chemicals were purchased from Sigma-Aldrich and Merck and used without any purification.

Instrumentation. Thorlabs fiber optic spectrometer CCS10 was used for Absorption and PL measurements. The power of the laser beam was measured using an Ophire Nova II powermeter. MDL-980 from CNI Laser was for used excitation. Zeiss EM900 was used for TEM imaging of the UCNPs.

Maskless Photolithography. Photolithography was performed using a Vivitek DX263 3500-Lumen XGA DLP Projector. Security surfaces were prepared by mixing 38 mg/ml colloidal solutions of each of the UCNPs in the photoresist matrix with a volume ratio of 1:2. Subsequently, the nanocomposite was kept in a desiccator for a time span of 24 h to remove its solvent. Glass slides were sonicated in acetone and isopropanol solvents and dried using a nitrogen gun. Each glass substrates was treated with 20 μL of Primer solution for enhancing the adhesion of the photoresist and afterward 500 μL of UV-3020 injected onto the surface. The prepared patterns were projected onto the sample for an optimum time span of 20 s and afterward development was carried out using an abundance of acetone. Finally the samples were rinsed with isopropanol and dried using a nitrogen gun.

Conflicts of interest

There are no conflicts to declare.

Acknowledgements

The authors are grateful for the technical and administrative support of the staff at Kharazmi University.

References

1. Auzel, F. Compteur Quantique par Transfert D'énergie Entre Deux Ions de Terres Rares Dans un Tungstate Mixte et Dans un Verre. *Comptes rendus de l'Académie des Sciences, Ser. B* **1966**, *262,* 1016-1019.
2. Ovsyankin, V. V.; P. P. Feofilov Mechanism of Summation of Electronic Excitations in Activated Crystals. *JETP Lett*. **1966**, *3,* 322-323.
3. Auzel, F. Upconversion and Anti-stokes Processes with f and d Ions in Solids. *Chem. Rev.* **2004**, *104*, 139-173.
4. Menyuk, N.; Dwight, K.; Pierce, J. W. $NaYF_4$:Yb,Er an Efficient Upconversion Phosphor. *Appl. Phys. Lett*. **1972**, *21*, 159-161.
5. Krämer, K. W.; Biner, D.; Frei, G.; Güdel, H. U.; Hehlen, M. P.; Lüthi, S. R. Hexagonal Sodium Yttrium Fluoride Based Green and Blue Emitting Upconversion Phosphors. *Chem. Mater*. **2004**, *16*, 1244-1251.
6. Wang, F.; Liu, X. Upconversion Multicolor Fine-tuning: Visible to Near-infrared Emission From Lanthanide-doped NAYF4 Nanoparticles. *J. Am. Chem. Soc*. **2008**, *130*, 5642-5643.
7. Haase, M.; Schäfer, H. Upconverting Nanoparticles, *Angew. Chem. Int. Ed*. **2011**, *50*, 5808-5829.
8. Boyer, J. C.; Vetrone, F.; Cuccia, L. A.; Capobianco, J. A. Synthesis of Colloidal Upconverting NaYF4 Nanocrystals Doped With Er^{3+},Yb^{3+} and Tm^{3+},Yb^{3+} via Thermal Decomposition of Lanthanide Trifluoroacetate Precursors. *J. Am. Chem. Soc*. **2006**, *128*, 7444-7445.
9. Rillings, K. W.; Roberts, J. E. A Thermal Study of the Trifluoroacetates and Pentafluoropropionates of Praseodymium, Samarium and Erbium. *Thermochim. Acta* **1974**, *10,* 285-298.
10. Rondeau, R. E.; Sievers, R. E. New Superior Paramagnetic Shift Reagents for Nuclear Magnetic Resonance Spectral Clarification. *J. Am. Chem. Soc*. **1971**, *93*, 1522-1524.
11. AltaVilla, C. *Upconverting Nanomaterials, Perspectives, Synthesis and Application*, CRC Press, Taylor & Francis: Boca Raton, FL, **2017**, 19-34.
12. Lee, J.; Bisso, P. W.; Srinivas, R. L.; Kim, J. J.; Swiston, A. J.; Doyle, P. S. Universal Process-Inert Encoding Architecture for Polymer Microparticles. *Nat. Mater.* **2014**, *13*, 524-529.
13. Heydari, E.; Sperling, J. R.; Neale, S. L.; Clark, A. W. Plasmonic Color Filters as Dual-state Nanopixels for High-density Microimage Encoding. *Adv. Funct. Mater.* **2017**, *27*, 1-6.
14. Huang, K.; Idris, N. M.; Zhang, Y.; Engineering of Lanthanide-Doped Upconversion Nanoparticles for Optical Encoding. *Small* **2015**, *12*, 836-852.
15. Meruga, J. M.; Cross, W. M.; May, P. S.; Luu, Qu.; Crawford, G. A.; Kellar, J. J. Security Printing of Covert Quick Response Codes Using Upconverting Nanoparticle Inks. *Nanotechnology* **2012**, *23*, 395201, 1-9.
16. You, M.; Lin, M.; Wang, S.; Wang, X.; Zhang, G.; Hong, Y.; Dong, Y.; Jin, G.; Xu, F. Three-Dimensional Quick Response Code based on Inkjet Printing of Upconversion Fluorescence Nanoparticles for Drug Anti-Counterfeiting. *Nanoscale* **2016**, *8*, 10096-100104.
17. Ma, Q.; Wang, J.; Li, Z.; Wang, D.; Hu, X.; Xu, Y.; Yuan, Q. Near Infrared light-mediated Photoactivation of Cytotoxic Re(i) Complexes by Using Lanthanide-doped Upconversion Nanoparticles. *Inorg. Chem. Front*. **2016**, *45*, 14101-14108.

18.Kim, W. J.; Nyk, M.; Prasad, P. N. Color-coded Multilayer Photopatterned Microstructures Using Lanthanide (III) Ion Co-doped NaYF4 Nanoparticles With Upconversion Luminescence for Possible Applications in Security. Nanotechnology 2009, 20, 185301, 1-7.

19.Wang, F.; Liu, X. Upconversion Multicolor Fine-Tuning: Visible to Near-Infrared Emission from Lanthanide-Doped $NaYF_4$ Nanoparticles. *J. Am. Chem. Soc.* **2008**, *130*, 5642-5643.

20.Mai, H.; Zhang, Y.; Sun, L.; Yan, C. Highly Efficient Multicolor Up-Conversion Emissions and Their Mechanisms of Monodisperse $NaYF_4$:Yb,Er Core and Core/Shell-Structured Nanocrystals. *J. Phys. Chem. C* **2007**, *111*, 13721-13729.

21.Boyer, J.; Cuccia, L. A.; Capobianco, J. A. Synthesis of colloidal upconverting NaYF4: Er^{3+}/Yb^{3+} and Tm^{3+}/Yb^{3+} monodisperse nanocrystals. *Nano Lett.*, **2007**,*7* , 847–852.

22.Boyer, J.; Vetrone, F.; Cuccia, L. A.; Capobianco, J. A. Synthesis of Colloidal Upconverting NaYF4:Er^{3+}/Yb^{3+} and Tm^{3+}/Yb^{3+} Monodisperse Nanocrystals. *J. Am. Chem. Soc.* **2006**, *128*, 7444-7445.

23.Zeng, J. H.; Su, J.; Li, Z. H.; Yan, R. X.; Li, Y. D. Synthesis and Upconversion Luminescence of Hexagonal−Phase $NaYF_4$:Yb, Er^{3+} Phosphors of Controlled Size and Morphology. *Adv. Mater.* **2005**, *17*, 2119-2123.

24.Yi, G. S.; Chow, G. M. Water-Soluble $NaYF_4$:Yb,Er(Tm)/$NaYF_4$/Polymer Core/Shell/Shell Nanoparticles with Significant Enhancement of Upconversion Fluorescence. *Chem. Mater.* **2007**, *19*, 341-343.

25.Li, Z.; Zhang, Y. An Efficient and User-friendly Method for the Synthesis of Hexagonal-phase $NaYF_4$:Yb,Er/Tm Nanocrystals with Controllable Shape and Upconversion Fluorescence. *Nanotechnology* **2008**, *19*, 345606,1-5.

26.Yi, G. S.; Chow, G. M. Synthesis of Hexagonal−Phase $NaYF_4$:Yb,Er and $NaYF_4$:Yb,Tm Nanocrystals with Efficient Up−Conversion Fluorescence. *Adv. Funct. Mater.* **2006**, *16*, 2324-2329.

27.Wu, S.; Butt, H. J. Near−Infrared−Sensitive Materials Based on Upconverting Nanoparticles. *Adv. Mater.* **2016**, *28*, 1208–1226.

28.Brites, C. D. S.; Lima, P. P.; Silva, N. J. O.; Millan, A.; Amaral, V. S.; Palacio, F.; Carlos, L. D. Thermometry at the Nanoscale. *Nanoscale* **2012**, *4*, 4799-4829.

29.Suyver, J. F.; Grimm, J.; Krämer, K.W.; Güdel, H. U. Highly Efficient Near-infrared to Visible Up-conversion Process in $NaYF_4$:Er^{3+},Yb^{3+}. *J. Lumin* **2005**, 114, 53-59.

30.Sedlmeier, A.; Achatz, D. E.; Fischer, L. H.; Gorris, H. H., Wolfbeis, O. S., Photon Upconverting Nanoparticles for Luminescent Sensing of Temperature. *Nanoscale* **2012**, *4*, 7090-7096.

31.Fischer, L. H.; Harms, G. S.; Wolfbeis, O. S. Upconverting Nanoparticles for Nanoscale Thermometry. *Angew. Chem. Int. Ed.* **2011**, *50*, 4546-4551.

32.Vetrone, F.; Naccache, R.; Zamarron, A.; Juarranz de la Fuente, A.; Sanz-Rodrıguez F.; Maestro L. M.; Rodriguez, E. M.; Jaque D.; Garcıa Sole, J.; Capobianco, J. A. Temperature Sensing Using Fluorescent Nanothermometers. *ACS Nano* **2010**, *4*, 3254-3258.

33.Zhou, S.; Deng, K.; Wei, X.; Jiang, G.; Duan, C.; Chen, Y.; Yin, M. Upconversion Luminescence of $NaYF_4$: Yb^{3+}, Er^{3+} for Temperature Sensing. *Opt. Commun.* **2013**, *291,* 138-142.

34. Dong, H.; Sun, L. -D.; Feng, W.; Gu, Y.; Li, F.; Yan, C.-H. Versatile Spectral and Lifetime Multiplexing Nanoplatform with Excitation Orthogonalized Upconversion Luminescence. *ACS Nano* **2017**, *11*, 3289-3297.
35. Deng, R.; Qin, F.; Chen, R.; Huang, W.; Hong, M.; Liu, X. Temporal Full-colour Tuning Through Non-steady-state Upconversion. *Nat. Nanotechnol.* **2015**, *10,* 237–242.

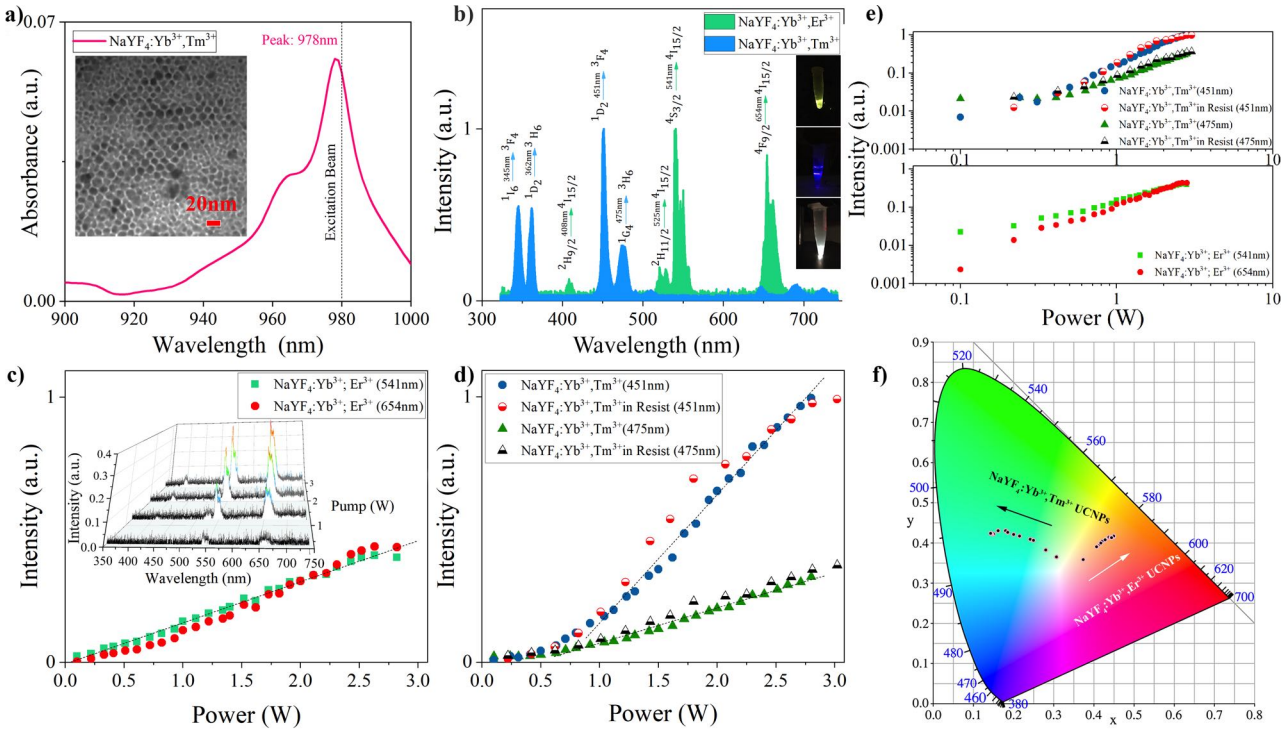

Figure 1. a) Absorption spectrum of the colloidal solution of $NaYF_4$:Yb^{3+},Tm^{3+} UCNPs in Hexane. Inset shows the TEM image of $NaYF_4$:Yb^{3+},Tm^{3+} UCNPs. b) PL of two UCNPs of NaYF4:Yb^{3+},Tm^{3+} in blue color and NaYF4: Yb^{3+}, Er^{3+} in green-yellow color. Inset from top to bottom shows the PL color of $NaYF_4$:Yb^{3+},Er^{3+} UCNPs, NaYF4:Yb^{3+},Tm^{3+} and their mixture. c) PL intensity of $NaYF_4$:Yb^{3+},Er^{3+} UCNPs versus excitation pump power for different peaks. Inset shows the PL development. d) PL intensity of $NaYF_4$:Yb^{3+},Tm^{3+} UCNPs in the hexane and photoresist versus excitation pump power for two blue color peaks. e) Logarithmic plot of PL intensity of $NaYF_4$:Yb^{3+},Er^{3+} and $NaYF_4$:Yb^{3+},Tm^{3+} UCNPs versus excitation pump. f) CIE1931 chromaticity diagram for both UC nanocomposites when the power of excitation laser is rising. White arrow is associated with $NaYF_4$:Yb^{3+},Er^{3+} UCNPs and the black arrow with $NaYF_4$:Yb^{3+},Tm^{3+} UCNPs.

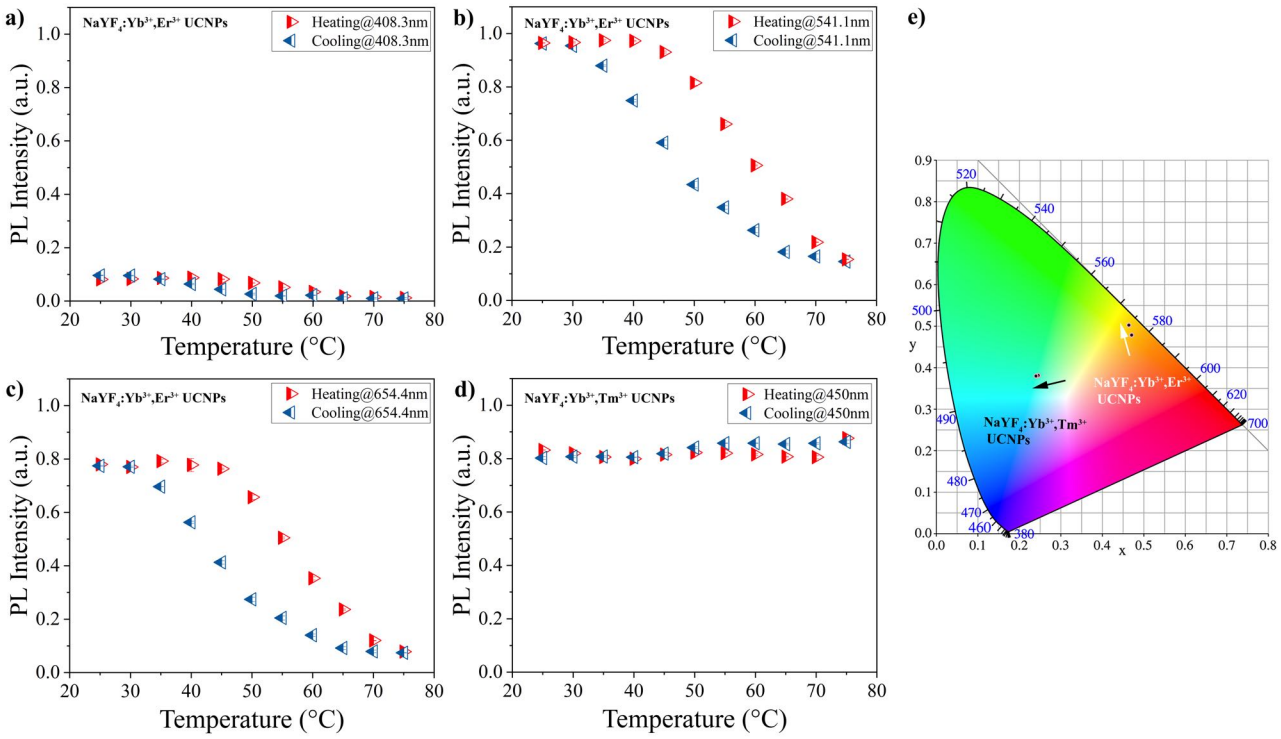

Figure 2. a) PL intensity versus temperature variation for $NaYF_4:Yb^{3+},Er^{3+}$ UCNPs at 408.3 nm. b) PL intensity versus temperature variation for $NaYF_4:Yb^{3+}$, Er^{3+} UCNPs at 541.1 nm. c) PL intensity versus temperature variation for $NaYF_4:Yb^{3+},Er^{3+}$ UCNPs at 654.4 nm d) PL intensity versus temperature for $NaYF_4:Yb^{3+},Tm^{3+}$ UCNPs at 451 nm e) CIE1931 chromaticity diagram shows the color change for two nanocomposites by changing the temperature.

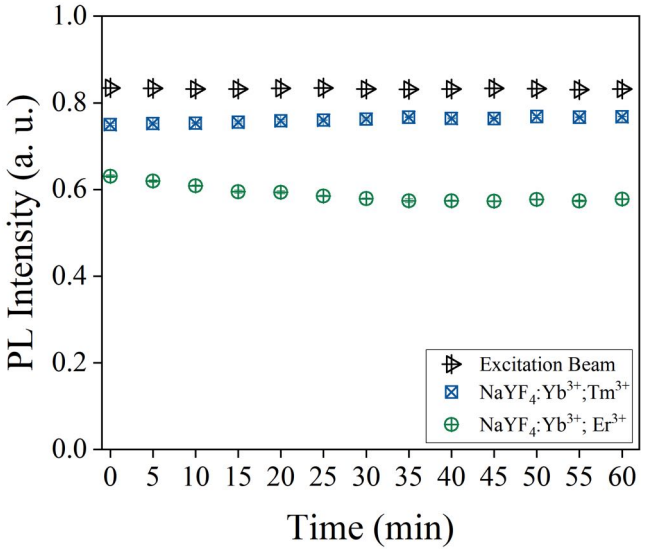

Figure 3. Long term stability test under 300 mW excitation laser beam with a spot size of 36 mm^2.

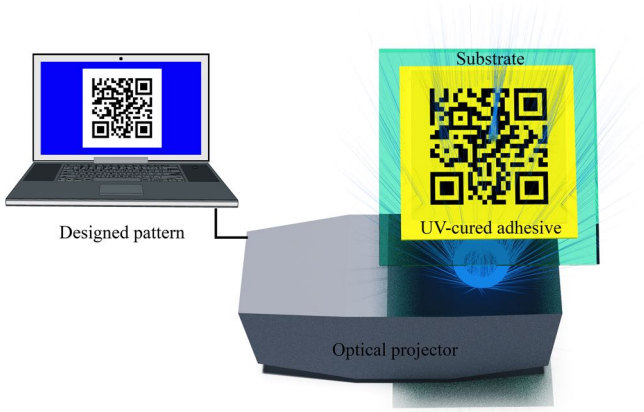

Figure 4. Maskless photolithography setup for fabrication of UCNP-doped security surfaces.

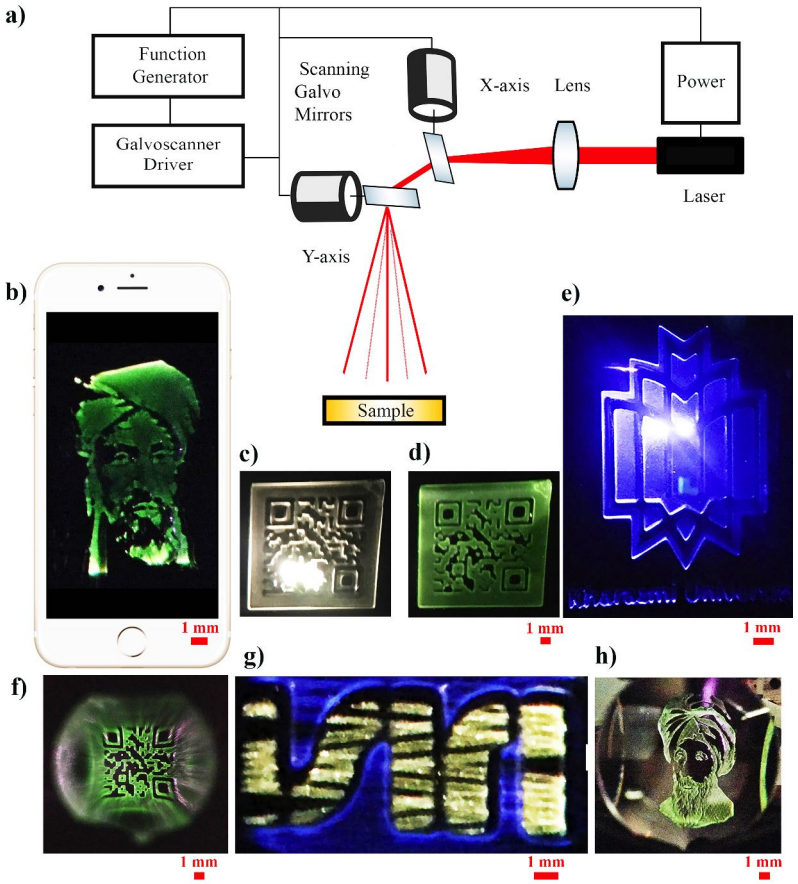

Figure 5: a) Optical setup for excitation and imaging of the patterned UC nanocomposites for security applications. b) Portrait of Kharazmi (Al-Khwarizmi) printed using a nanocompsite of $NaYF_4$:Yb^{3+},Er^{3+} UCNPs doped in the photoresist and recorded by a smartphone. c) A QR-code comprise of a blend of two UCNPs and excited with a static excitation laser beam. d) A QR-code comprise of a blend of two UCNPs and excited with a dynamic excitation laser beam e) Logo of the Kharazmi University comprised of $NaYF_4$:Yb^{3+},Tm^{3+} UCNPs doped in the photoresist. f) A QR-code comprised of $NaYF_4$:Yb^{3+},Er^{3+} UCNPs doped in the photoresist and captured throughout a convex lens with 5 cm focal length. g) A two-color pattern fabricated by a two-step maskless photolithography. h) Portrait of Ibn Al-haytham comprised of $NaYF_4$:Yb^{3+},Er^{3+} UCNPs doped in the photoresist and captured throughout a convex lens with 5 cm focal length.